Singer, B.S., Jicha, B.R., Sawyer, D., Walaszczyk, I., Buchwaldt, R., and Mutterlose, J., 2020, Geochronology of late Albian–Cenomanian strata in the U.S. Western Interior: GSA Bulletin, https://doi.org/10.1130/B35794.1.

Supplemental Material

Figure S1. Stratigraphic nomenclature and correlation chart, modified from MacKenzie (1965), shows new ages in a series of columns, with assumed named correlations showing mismatch in determined ages.

Figure S2. GoogleEarth oblique image with location of bentonite sample 90-O-51, the local topmost bentonite in the Mowry Shale, section 28, Township 42N, Range 81W, Jefferson County, Wyoming, collected by W.A. Cobban & E.A. Merewether.

Figure S3. (A). Plate 1 modified from Reeside and Cobban (1960). (B). Measured section at Shell Creek by W.A. Cobban and E.A. Merewether. New radioisotopic ages and fossil occurrences are illustrated to provide context.

Figure S4. Annotated Plate 4 of Robinson et al. (1964), illustrating the complex discontinuity of bentonites and sandstone lenses in the Newcastle Sandstone.

Figure S5. Stratigraphic section from Soap Creek Dome, Crow Indian Reservation, Montana, showing bentonites sampled by W.A. Cobban and J.D. Obradovich. This section likely straddles the Albian-Cenomanian Boundary, and contains all three inoceramid zones: lower *Gnesioceramus comancheanus*, intermediate *Posidonioceramus nahwisi* zone, and upper *Gnesioceramus mowriensis* zone (Walaszczyk and Cobban, 2016).

Figure S6. (A). Index figure for the Wind River Basin, Wyoming modified from from Finn (2017), showing new ages located by section-range-township within and adjoining the Wind River Basin. (B). Stratigraphic sections and paleogeographic map from Dresser (1974) report on the Muddy Sandstone around the Wind River Basin. (C). Dual Induction Focused-Gamma Ray log for Pacific Enterprises Dishpan Federal 12-29, 2931n95w_SwNw, API #13-21633, showing part of log from upper Thermopolis Shale to lower Mowry Shale, modifed from Finn (2017).

Figure S7. Composite modified from of Figures 7 and 10 from Cobban et al. (1976). The Lower Taft Hill Member is biostratigraphically *Gnesioceramus comancheanus* (*G. bellvuensis*) in age, and has a bentonite age from upper unit dated at 103.08 ± 0.03/0.11/0.20 Ma; the overlying Vaughn Member has a dated bentonite at 102.68 ± 0.03/0.07/0.18 Ma.

Figure S8. Photograph (facing southeast) of sample locations for U-Pb zircon ages at the Alameda Roadcut, Dinosaur Ridge, Colorado, in the Dakota "J" Sandstone (Kassler Member, KJ08161) 104.02 ± 0.04 Ma and underlying Skull Creek Shale (KJ08160) 104.69 ± 0.05 Ma. Sample KJ08162 103.92 ± 0.04 Ma is from the north side of the road, from a thin volcanic ash bed, also in the Kassler Member. Photo by Robert Buchwaldt.

Figure S9. Index map of the Bighorn Basin, Wyoming and Montana modified from Finn (2014) USGS SIR 13-5138, showing ages located by section-range-township within and adjoining the

Bighorn Basin. New ages, sample numbers, and stratigraphic units are listed on the bottom of the map. In addition, significant type well (logs) and cores are indicated, including Intercontinental Federal 2, illustrated in Figure S10.

Figure S10. Dual Induction Shallow Focused-Gamma Ray log for Internorth Federal 2-32, 3254n94w_SeSe, API #03-20565, showing part of log from base of Thermopolis Shale to lower Frontier Formation, modified from Finn (2014). Dated bentontites from Central Wyoming, are projected into this section. Ages from the northern Bighorn Basin are closely related to the well log; sample locations projected from adjoining basins are italicized. Red lines show multiple bentonite horizons, especially in the Mowry Shale.

Figure S11. Google Earth image of northern Bighorn Basin, Greybull, Wyoming with locations anbd dates from bentonites from the Shell Creek Shale (99.67 ± 0.13 Ma); upper Thermopolis Shale (101.36 ± 0.11 Ma); and lower Thermopolis Shale (106.37 ± 0.11 Ma).

Figure S12. Oblique Google Earth images of Dinosaur Ridge, Alameda Roadcut, Dakota Sandstone U-Pb ages. (A) looking southwest toward Red Rocks, Jefferson County, west of Denver, Colorado. A close-up of south side sample locations is in Figure S8. (B) View to the North. (C) Close-up view to the Southwest. (D) Close-up view to the Northeast.

Figure S13. Oblique Google Earth view of Dakota Sandstone on Colorado Highway 115 at Deadman Canyon, south of Colorado Springs. The age of 99.37 ± 0.31 Ma, determined by John Obradovich, is from the lower Dry Creek Canyon Member (Oboh-Ikuenobe et al., 2008).

Figure S14. Middle Cenomanian ammonite/inoceramid faunas and recent age determinations in the the southeast San Juan Basin (Owen et al., 2007) and adjoining Laguna Pueblo area (Cobban, 1977).

Figure S15. Upper Cenomanian ammonite/inoceramid faunas and age determinations relavent in south central Utah, as documented by Elder, Gustason, and Sageman (1994).

Table S1. Complete $^{40}Ar/^{39}Ar$ results using the Noblesse mass spectrometer.

Table S2. Complete U-Pb isotopic data from zircons and concordia plots from Dakota Sandstone, Dinosaur Ridge, Jefferson County, Colorado.

Supplementary Materials. Figures providing context for location and stratigraphic positions of dated bentonites in:

Geochronology of late Albian- Cenomanian strata in the US Western Interior

Brad S. Singer, Brian R. Jicha, David Sawyer, Ireneusz Walaszczyk, Robert Buchwaldt, Jorg Mutterlose

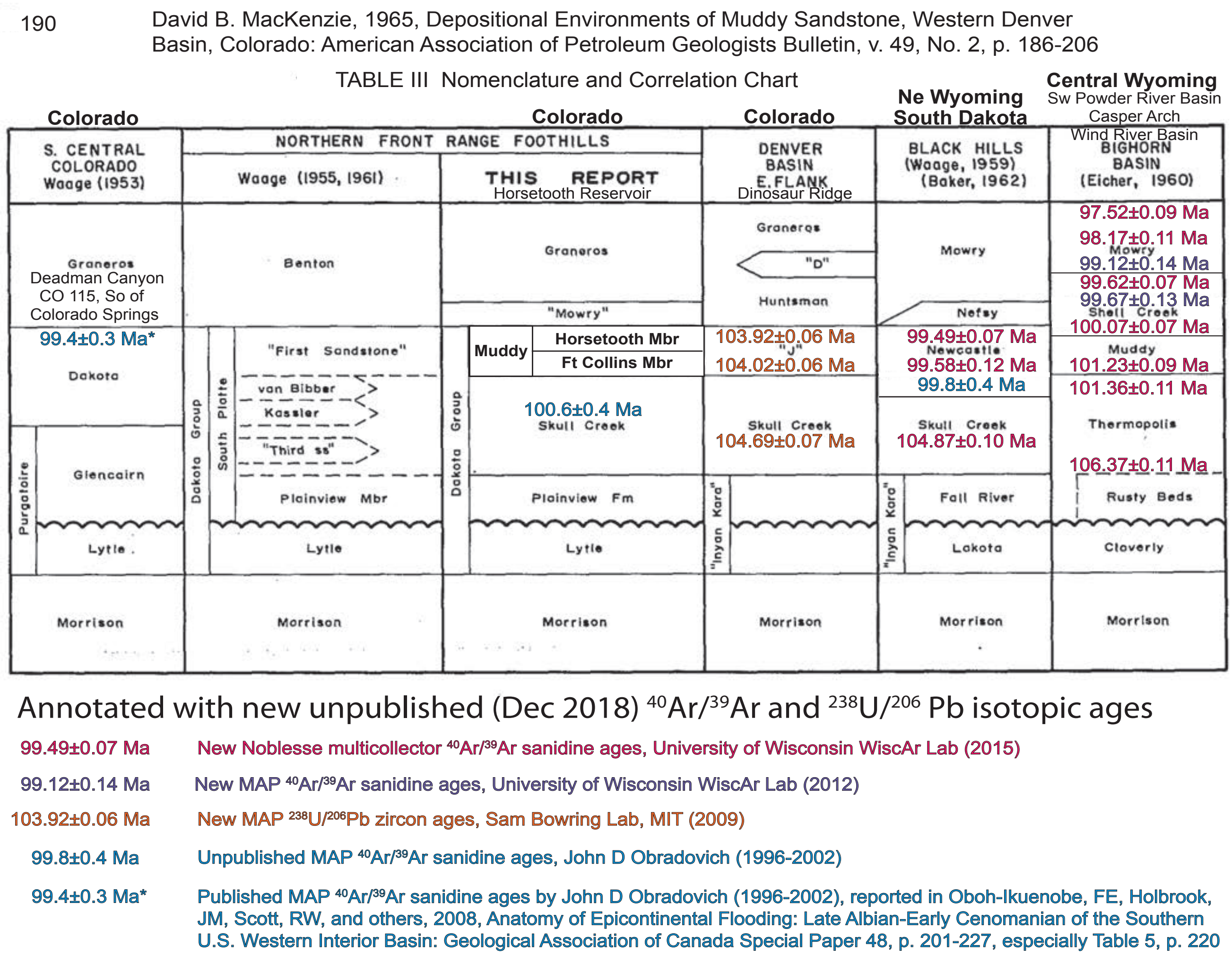

Figure S1. Stratigraphic nomenclature and correlation chart, modified from MacKenzie (1965), shows new ages in a series of columns, with assumed named correlations showing mismatch in determined ages. This chart highlights a Denver Basin, Colorado viewpoint for age and stratigraphic relations and can be compared to Figure 3 in our paper, which is centered more in the Powder River Basin and Wyoming. $^{40}Ar/^{39}Ar$ ages reported with $\pm 2\sigma$ analytical plus J value uncertainties.

Figure S2. GoogleEarth oblique image with the quarter-quarter section outline of bentonite sample 90-O-51, the local topmost bentonite in the Mowry Shale, section 28, Township 42N, Range 81W, Jefferson County, Wyoming, collected by W.A. Cobban & E.A. Merewether.

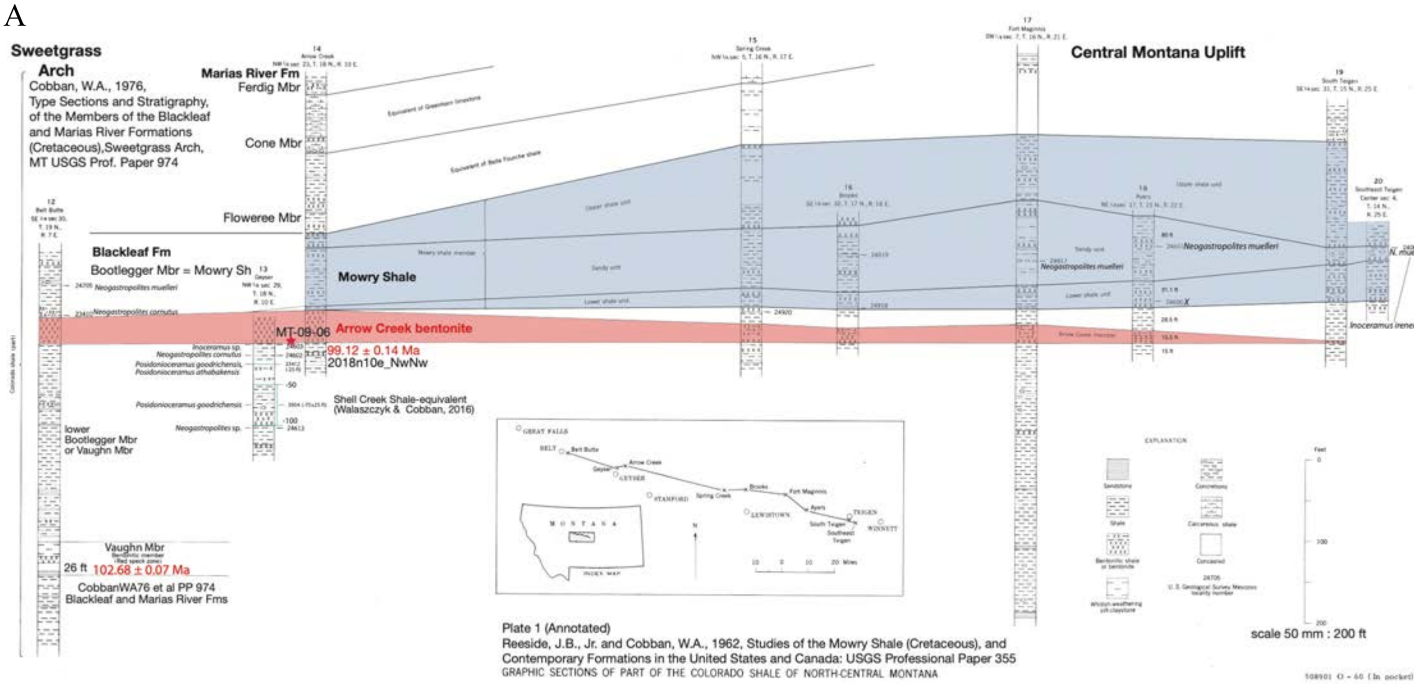

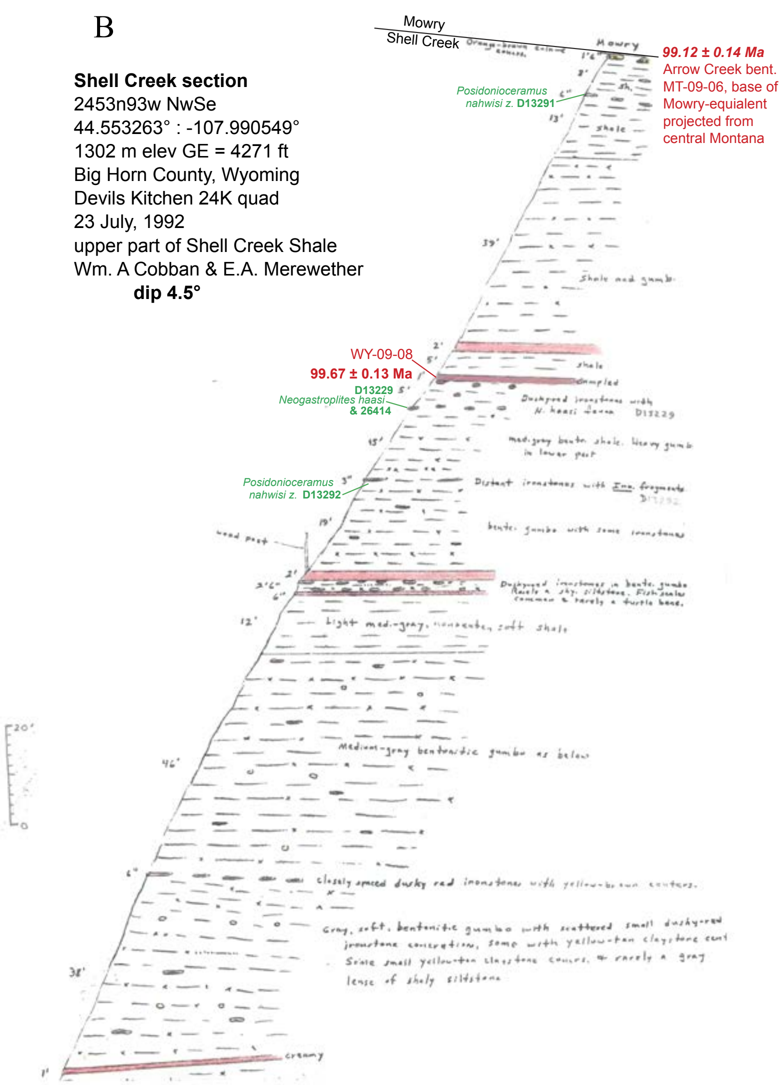

Figure S3. **(A).** Plate 1 modified from Reeside and Cobban (1960). At second column from left is the new age of 99.12 ± 0.10/0.14/0.21 Ma for the Arrow Creek bentonite, as it transitions from the Bootlegger Member of the Blackleaf Formation in the Sweetgrass Arch, to the base of the Mowry Shale in central Montana. Inoceramids (*Posidonioceramus goodrichensis*, *P. athabakensis*) and ammonite (*Neogastroplites cornutus*, *N. muelleri*) are shown relative to Arrow Creek bentonite marker. The Vaughan Member (102.68 ± 0.0/0.03/0.07/0.18 Ma) is projected from west of Great Falls, correlation from Vaughn to Belt Butte has not been not worked out with respect to Mowry-Bootlegger and Vaughn Member contacts; likely there is an unrecognized unconformity. **(B).** Measured section at Shell Creek by W.A. Cobban and E.A. Merewether, showing the upper Shell Creek Shale, with ammonite and inoceramid collections and corresponding location numbers. Bentonite dated at 99.67 ± 0.11/0.13/0.20 Ma is 5′ above *Neogastroplites haasi*, stratigraphically lowest ammonite in the U.S. Western Interior. Projected age of 99.12 ± 0.14 Ma is from central Montana, but the basal Mowry contact may stratigraphically rise or fall from the Sweetgrass Arch/Belt Butte, Montana to the Eastern Bighorn Basin, Wyoming (>500 km).

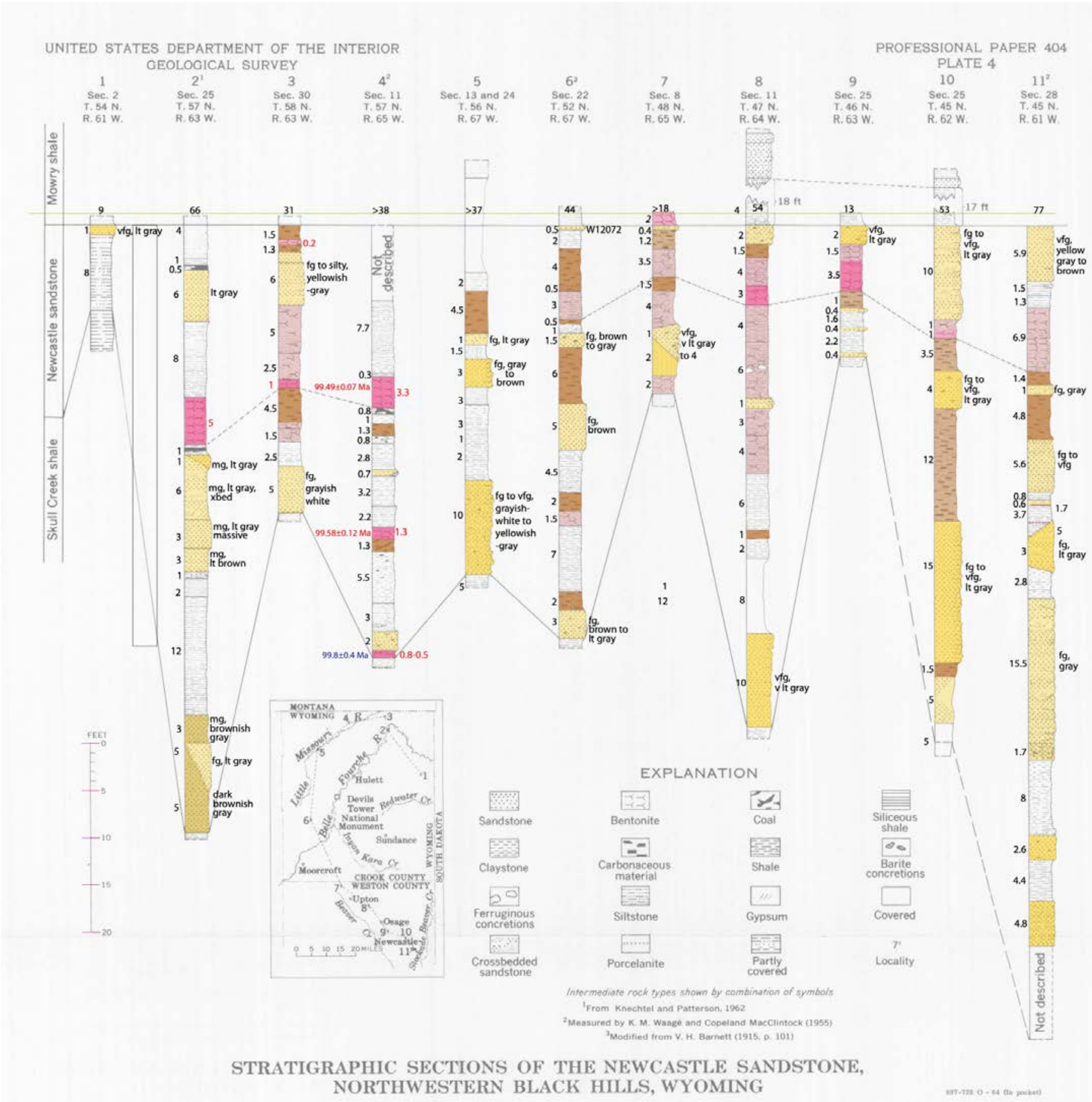

Figure S4. Annotated Plate 4 of Robinson et al. (1964), illustrating the complex discontinuity of bentonites and sandstone lenses in the Newcastle Sandstone. Bentonite ages from Strawberry Butte near Hulett, Wyoming are project to this northern perimeter line of section around northern Black Hills. 99.8 ± 0.4 Ma on the lowest bentonite in the Newcastle Sandstone is from J.D. Obradovich (personal communication), not analytically distinct.

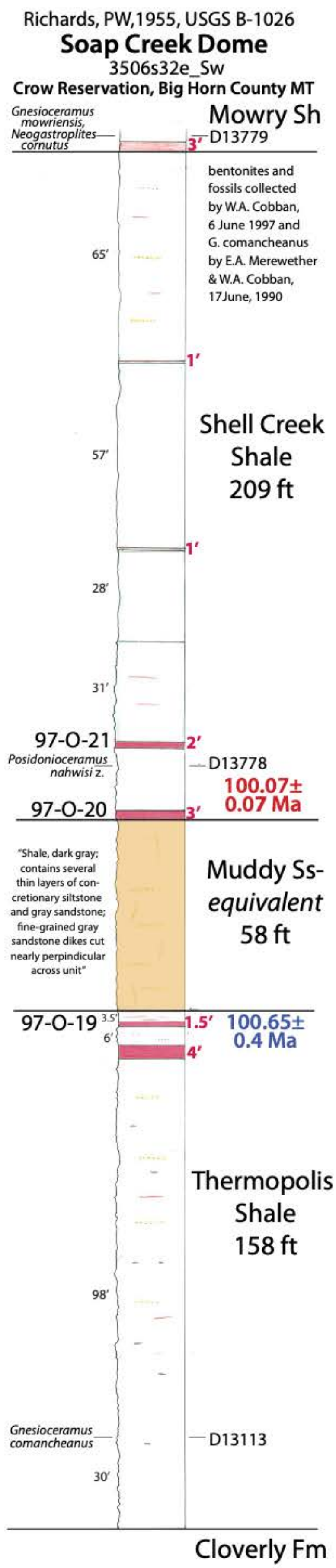

Figure S5. Stratigraphic section from Soap Creek Dome, Crow Indian Reservation, Montana, showing bentonites sampled by W.A. Cobban and J.D. Obradovich. A bentonite sample (97-O-20) from the basal Shell Creek Shale gives an age of 100.07 ± 0.07 Ma, whereas an age of 100.65 ± 0.4 Ma (Obradovich, personal communication) on the underlying 97-O-19 brackets a "Muddy Sandstone-equivalent" section, that consists of no more than several thin layers of concretionary siltstone and gray sandstone, set in dominant lithology of dark gray shale (Richards, 1955, p. 46). This section likely straddles the Albian-Cenomanian Boundary, and contains all three inoceramid zones: lower *Gnesioceramus comancheanus*, intermediate *Posidonioceramus nahwisi* zone, and upper *Gnesioceramus mowriensis* zone (Walaszczyk and Cobban, 2016).

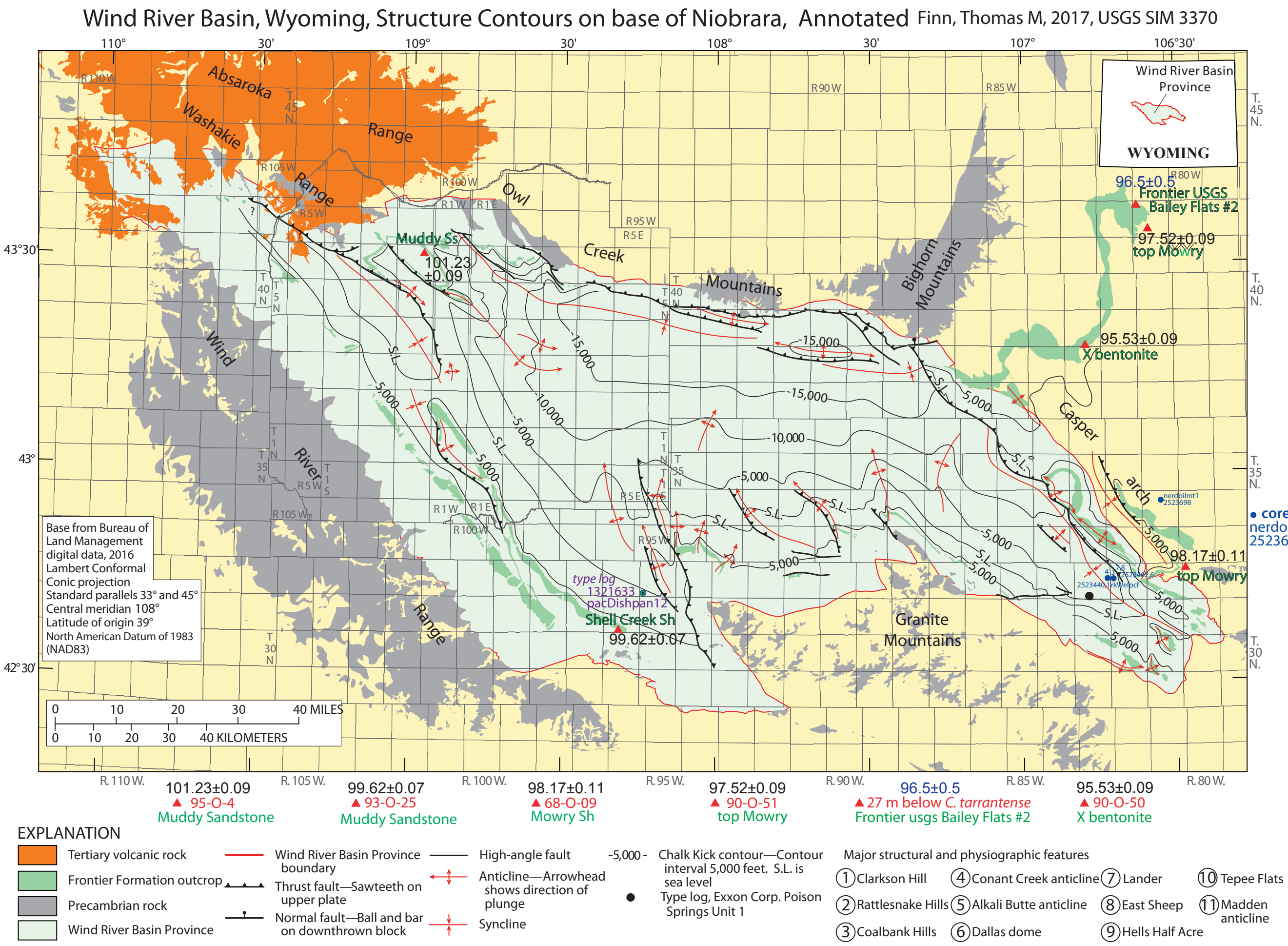

Figure 2. Index map of the Wind River Basin Province in central Wyoming showing major structural and physiographic features discussed in the text: (1) Clarkson Hill, (2) Rattlesnake Hills, (3) Coalbank Hills, (4) Conant Creek anticline, (5) Alkali Butte anticline, (6) Dallas dome, (7) Lander, (8) East Sheep Creek/Shotgun Butte, (9) Hells Half Acre, (10) Teepee Flats gas field, and (11) Madden anticline. Structure contours are drawn at base of the "chalk kick" marker bed. Contour interval is 5,000 feet. S.L., sea level.

Figure S6. (A). Index figure for the Wind River Basin, Wyoming modified from from Finn (2017), showing new ages located by section-range-township within and adjoining the Wind River Basin. Ages, sample numbers, and stratigraphic units are listed on the bottom of the map. In addition, significant type well (logs) and cores are indicated, including Pacific Dishpan 12, illustrated in **Fig. S6C**. $^{40}Ar/^{39}Ar$ ages reported with ± 2σ analytical plus J value uncertainties.

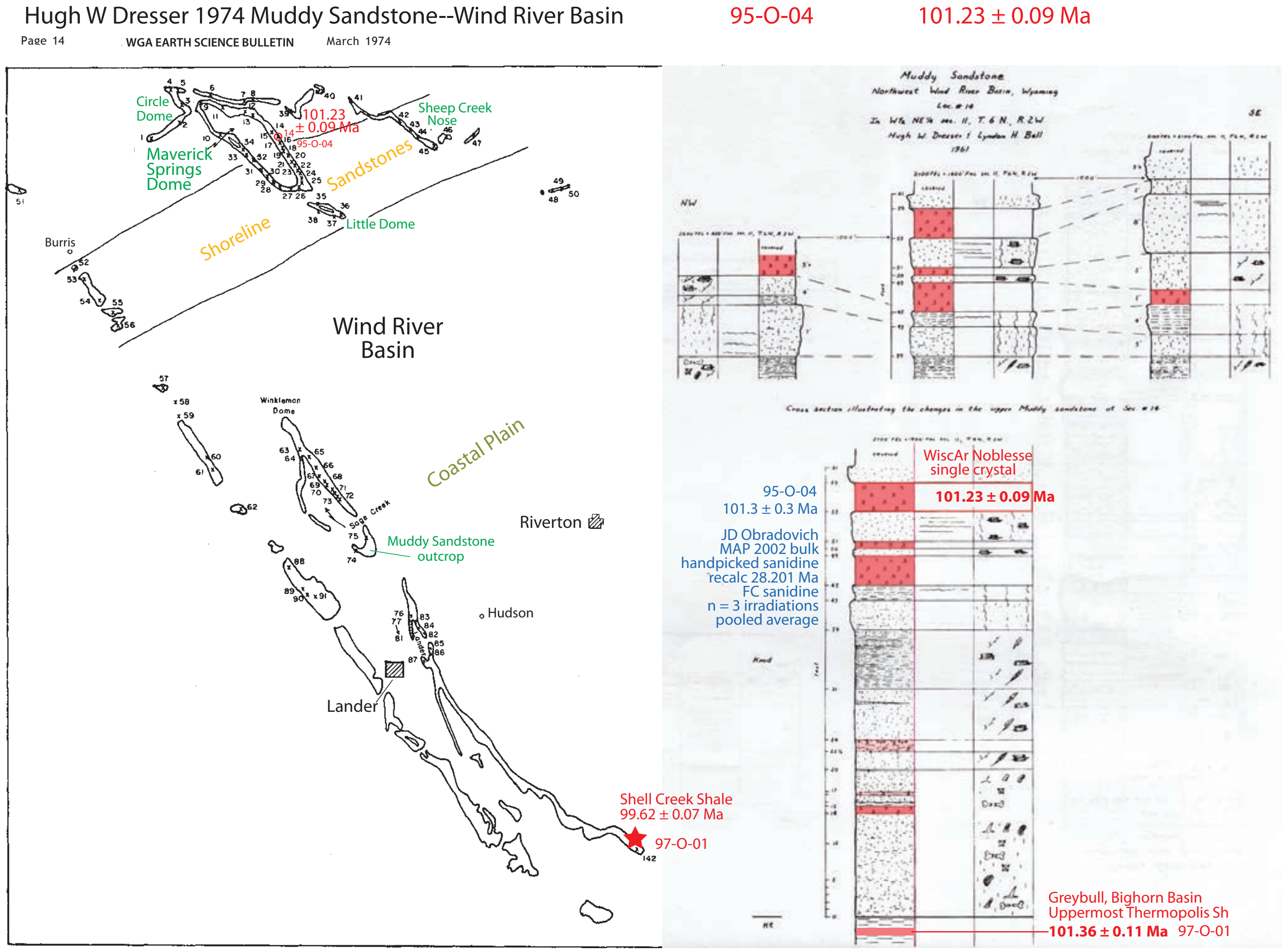

Figure S6. (B). Stratigraphic sections and paleogeographic map from Dresser (1974) report on the Muddy Sandstone around the Wind River Basin. The figure shows the location of the dated bentonite, on the northeast flank of the Maverick Springs Dome, in a shallow marine setting, just offshore from the shoreface sandstones. The stratigraphic column at locality 14 shows the dated bentonite, the uppermost of 2 upper bentonites; the cross-section above illustrates the discontinuity of bentonite horizons--1000 ft to either side, showing pinchout of the bentonites. Maverick Springs Dome is located within the Wind River Indian Reservation.

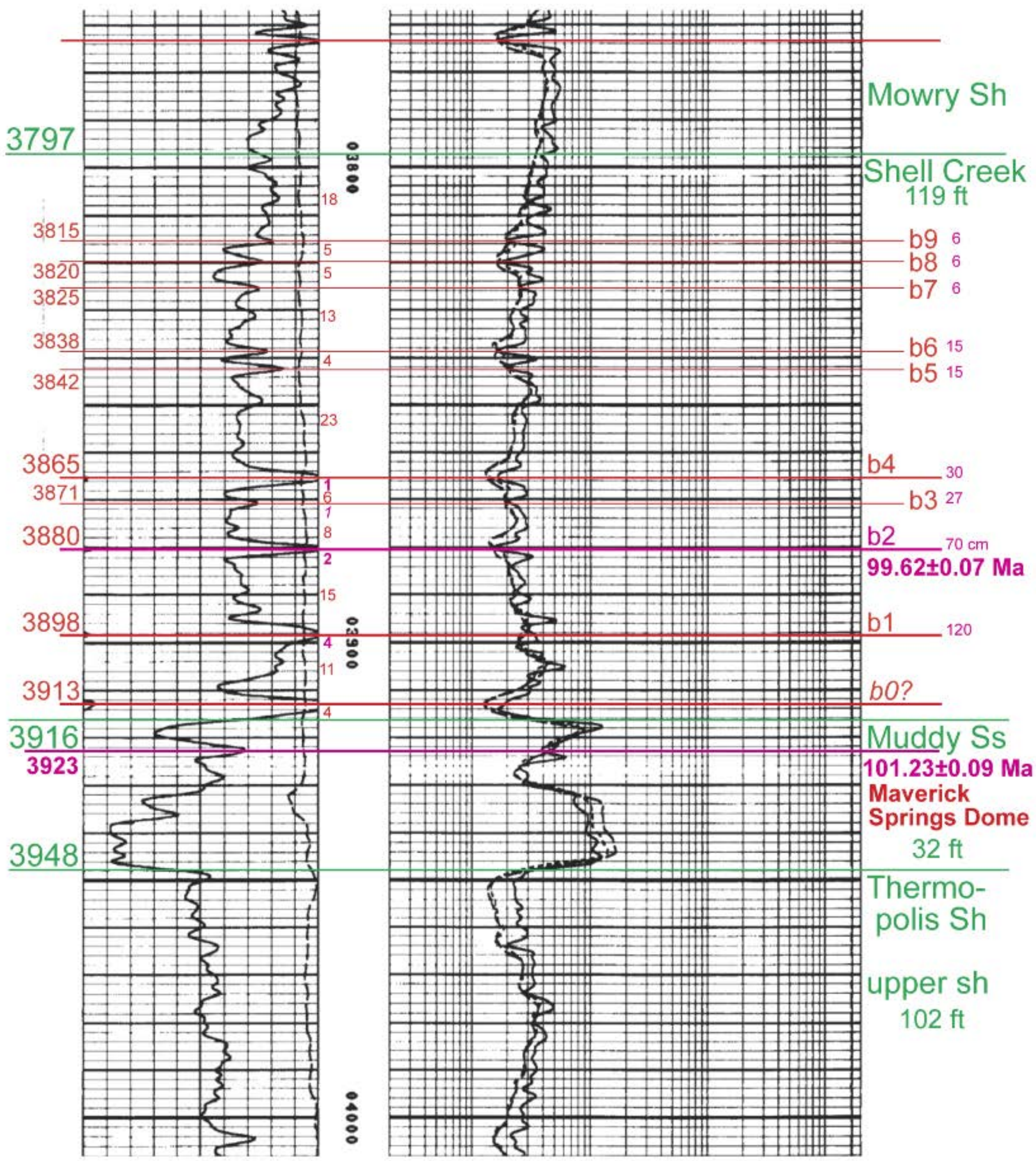

Figure S6. (C). Dual Induction Focused-Gamma Ray log for Pacific Enterprises Dishpan Federal 12-29, 2931n95w_SwNw, API #13-21633, showing part of log from upper Thermopolis Shale to lower Mowry Shale, modifed from Finn (2017). In western Wind River Basin, the Muddy Sandstone (32 ft) and overlying Shell Creek Shale (119 ft) have at least 12 bentonites marked (red), and include the nearby (9 km E) bentonite (b2) dated at 99.62 ± 0.04 Ma; the age of the Maverick Springs Dome Muddy Sandstone 101.23 ± 0.06 Ma is projected into section from 112 km north (for map location).

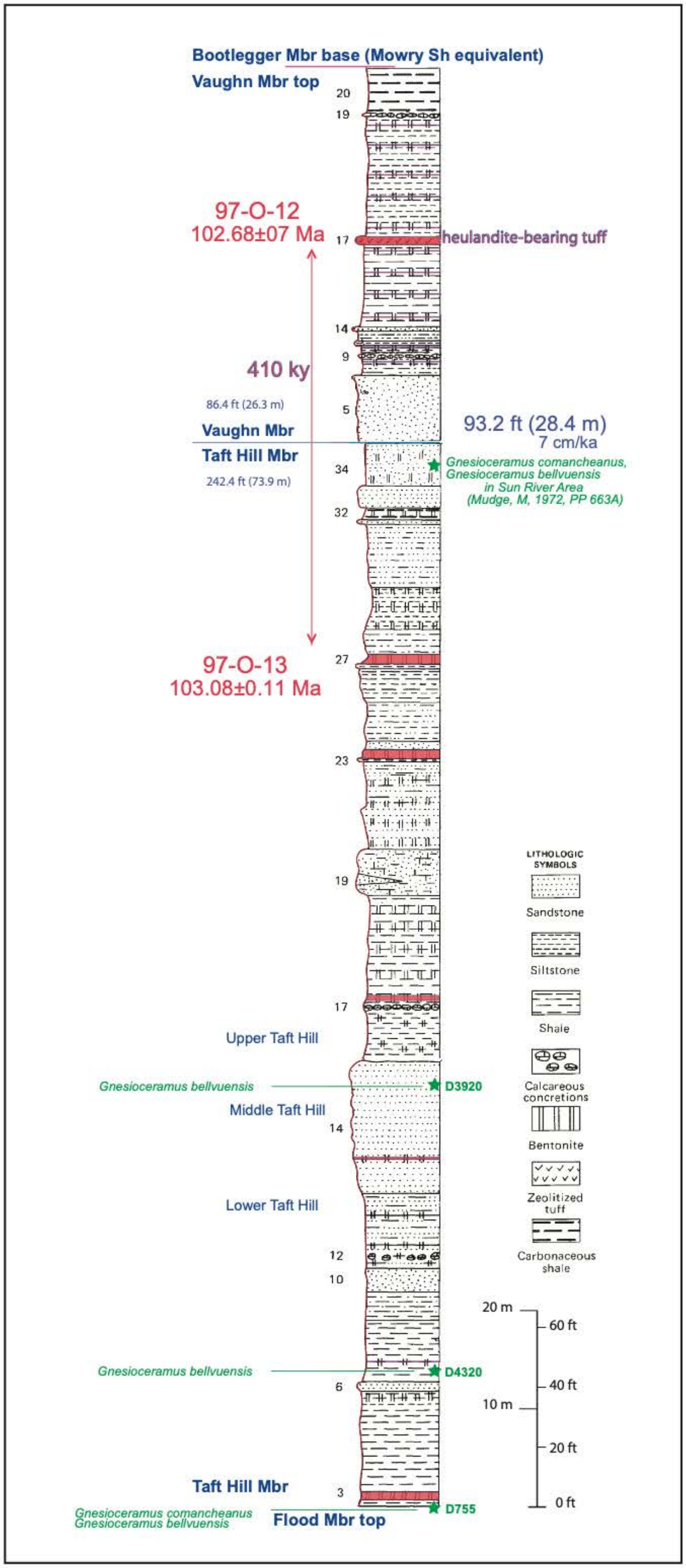

Figure S7. Composite modified from of Figures 7 and 10 from Cobban et al. (1976). The Lower Taft Hill Member is biostratigraphically *Gnesioceramus comancheanus* (*G. bellvuensis*) in age, and has a bentonite age from upper unit dated at 103.08 ± 0.03/0.11/0.20 Ma; the overlying Vaughn Member has a dated bentonite at 102.68 ± 0.03/0.07/0.18 Ma.

Figure S8. Photograph (facing southeast) of sample locations for U-Pb zircon ages at the Alameda Roadcut, Dinosaur Ridge, Colorado, in the Dakota "J" Sandstone (Kassler Member, KJ08161) 104.02 ± 0.04 Ma and underlying Skull Creek Shale (KJ08160) 104.69 ± 0.05 Ma. Sample KJ08162 103.92 ± 0.04 Ma is from the north side of the road, from a thin volcanic ash bed, also in the Kassler Member. Photo by Robert Buchwaldt.

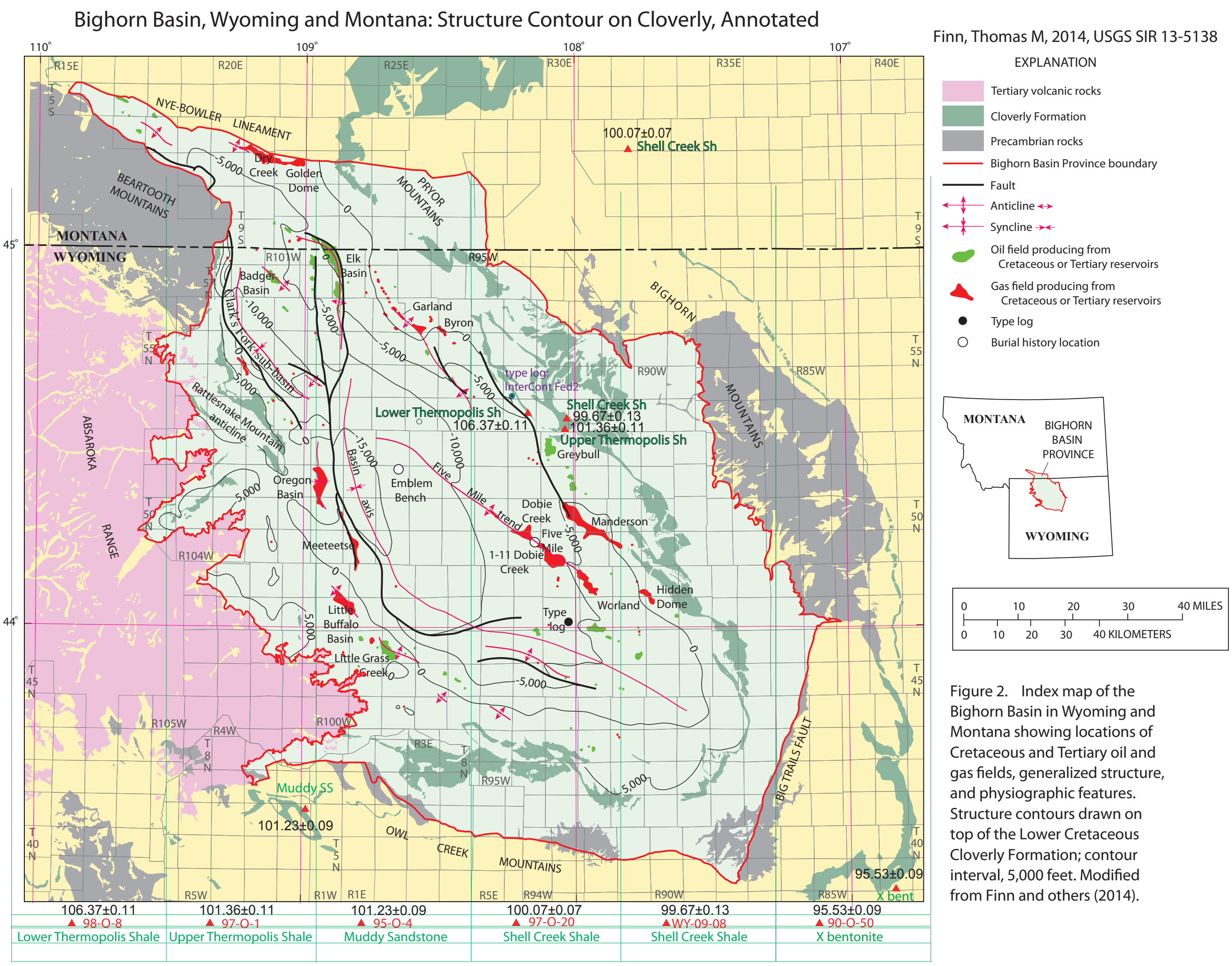

Figure S9. Index map of the Bighorn Basin, Wyoming and Montana modified from Finn (2014) USGS SIR 13-5138, showing ages located by section-range-township within and adjoining the Bighorn Basin. New ages, sample numbers, and stratigraphic units are listed on the bottom of the map. In addition, significant type well (logs) and cores are indicated, including Intercontinental Federal 2, illustrated in **Figure S10**.

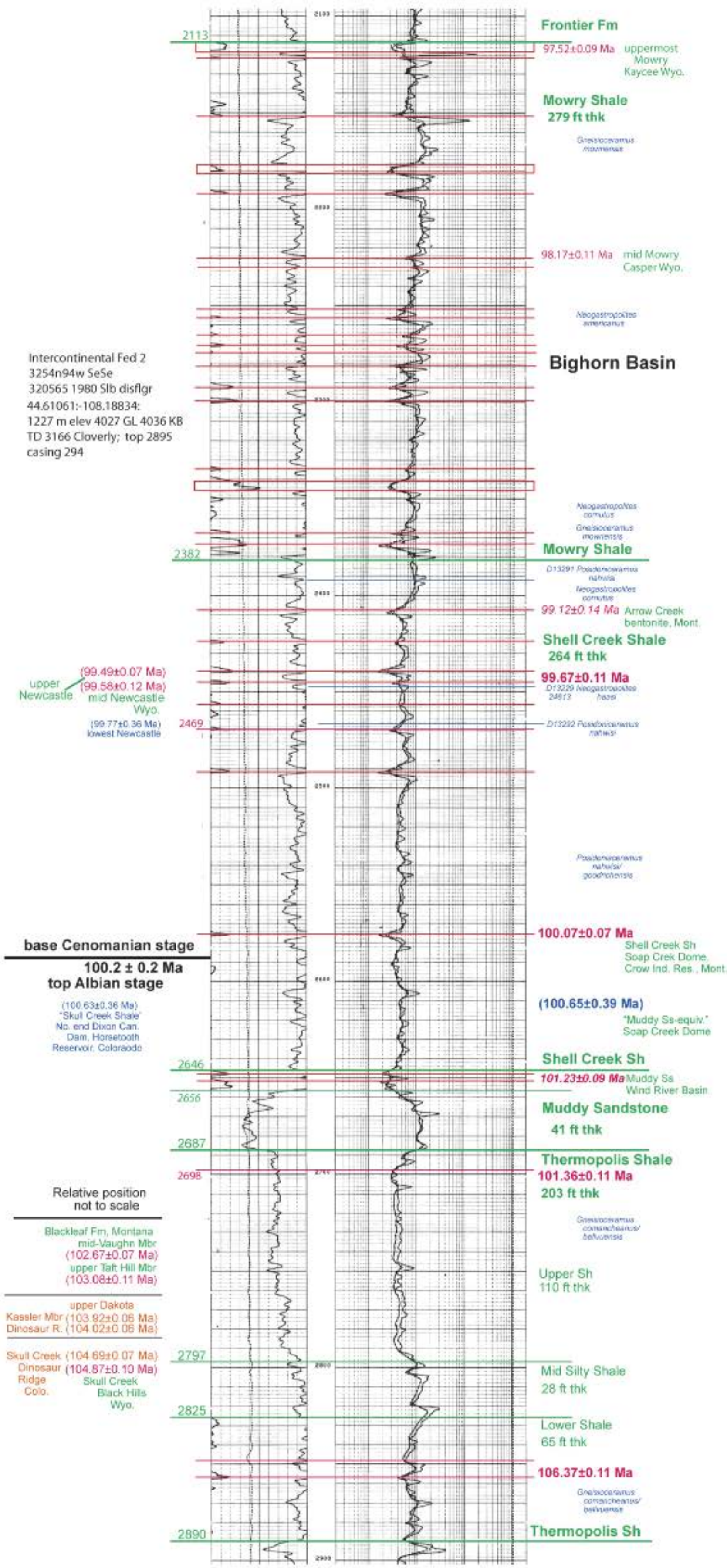

Figure S10. Dual Induction Shallow Focused-Gamma Ray log for Internorth Federal 2-32, 3254n94w_SeSe, API #03-20565, showing part of log from base of Thermopolis Shale to lower Frontier Formation, modified from Finn (2014). All the dated bentontites from (No) Central Wyoming (Bighorn and Wind River Basins, and the Casper Arch), are projected into this section. Ages from the northern Bighorn Basin are closely related to the well log; sample locations projected from adjoining basins are italicized. Red lines show multiple bentonite horizons, especially in the Mowry Shale. $^{40}Ar/^{39}Ar$ ages reported with $\pm$ 2σ analytical plus J value uncertainties.

Figure S11. Google Earth image of northern Bighorn Basin, Greybull, Wyoming. Locations are shown for the dated bentonites from the Shell Creek Shale (99.67 ± 0.13 Ma); upper Thermopolis Shale (101.36 ± 0.11 Ma); and lower Thermopolis Shale (106.37 ± 0.11 Ma). Location for the type log for the Bighorn Basin illustrated in **Figure S10** is found northwest of the Lower Thermopolis Shale age locality. Sheep Mountain Anticline, highlighted by the orange Chugwater Formation is conspicuous to the north of Greybull. $^{40}Ar/^{39}Ar$ ages reported with ± 2σ analytical plus J value uncertainties.

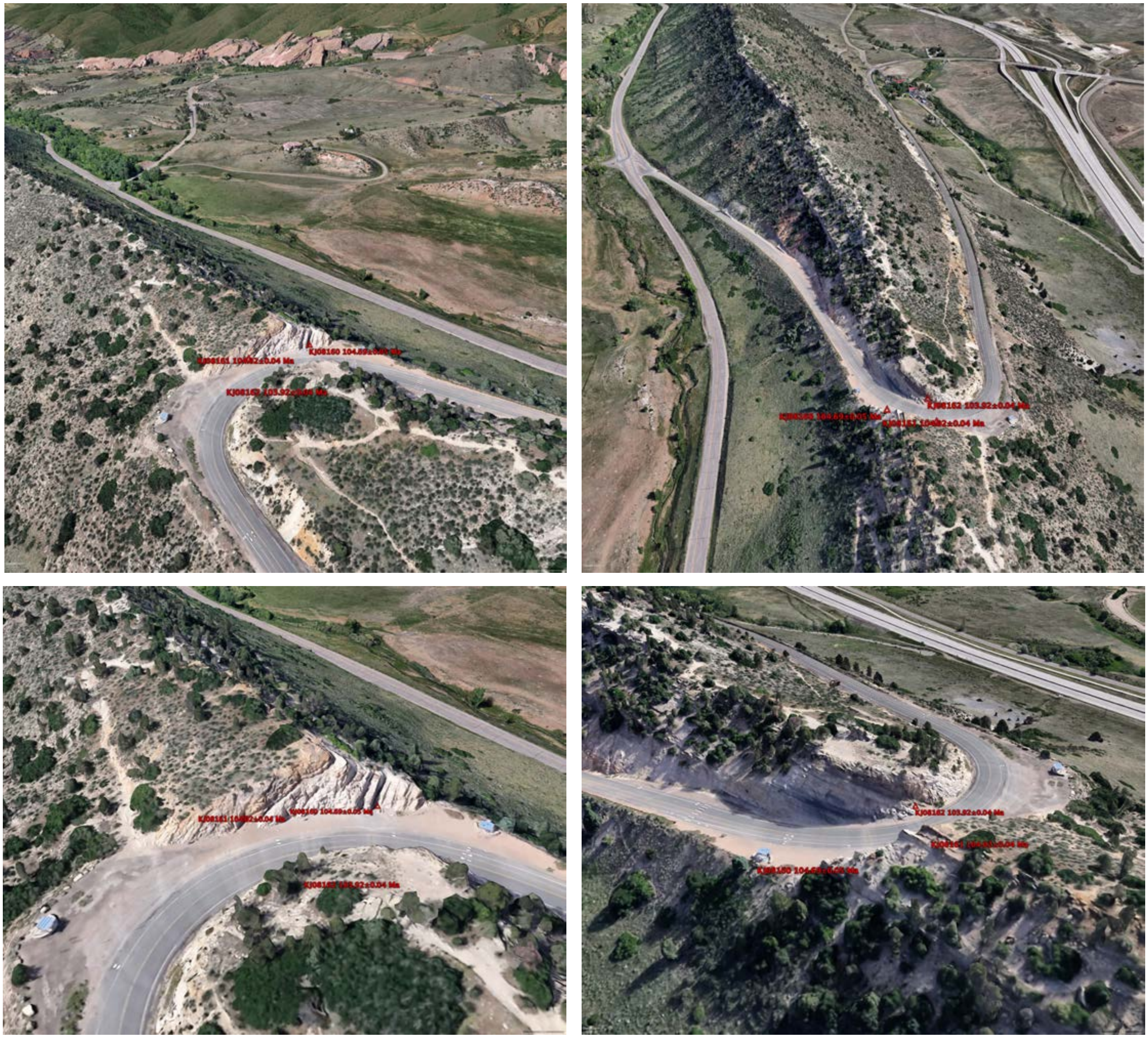

Figure S12. Oblique Google Earth images of Dinosaur Ridge, Alameda Roadcut, Dakota Sandstone U-Pb ages. **A**. looking southwest toward Red Rocks, Jefferson County, west of Denver, Colorado. A close-up of south side sample locations is in **Figure S8**. **B**. View to the North. **C.** Close-up view to the Southwest. **D**. Close-up view to the Northeast.

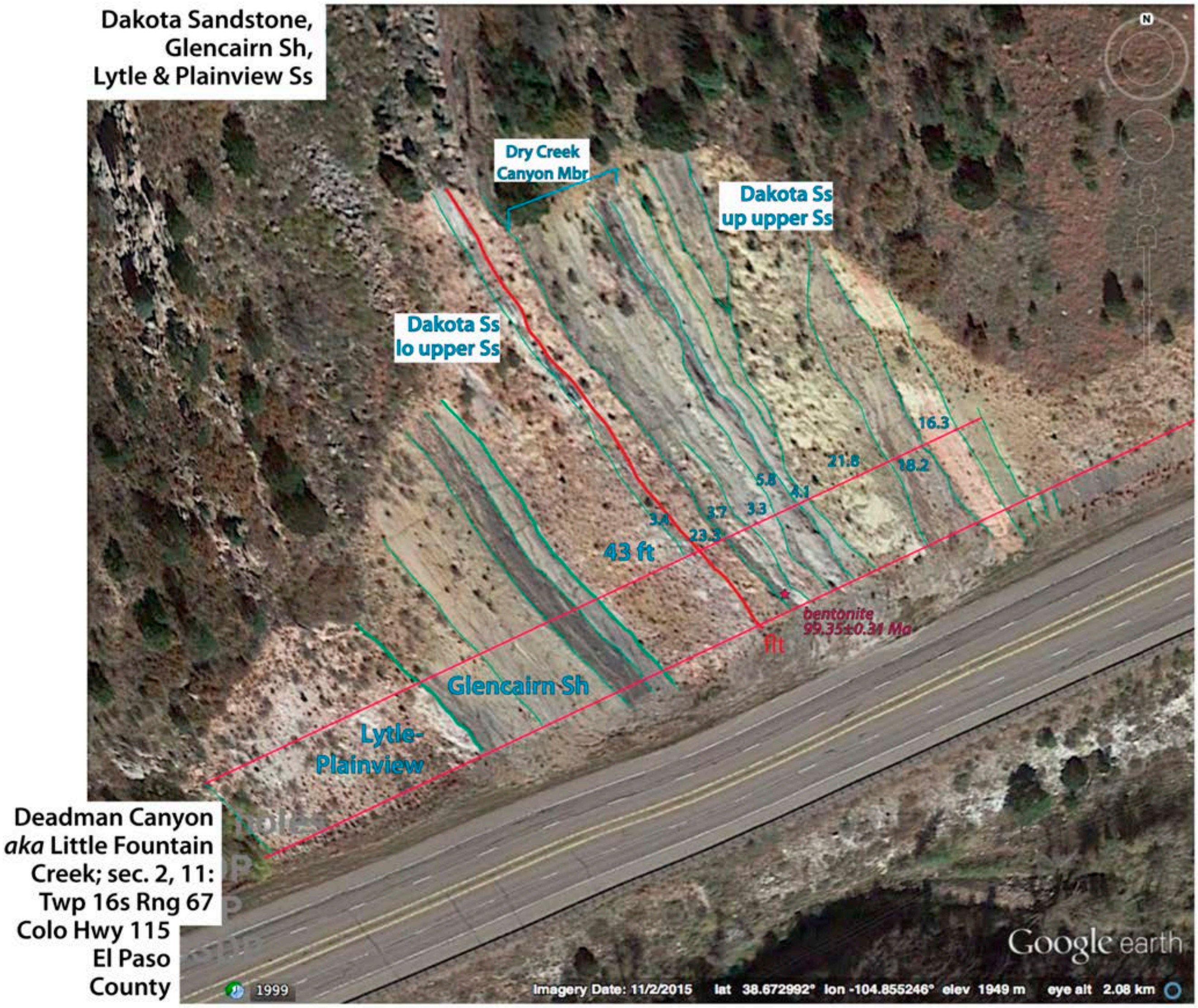

Figure S13. Oblique Google Earth view of Dakota Sandstone on Colorado Highway 115 at Deadman Canyon, south of Colorado Springs. The age of 99.37 ± 0.31 Ma, determined by John Obradovich, is from the lower Dry Creek Canyon Member (Oboh-Ikuenobe et al., 2008).

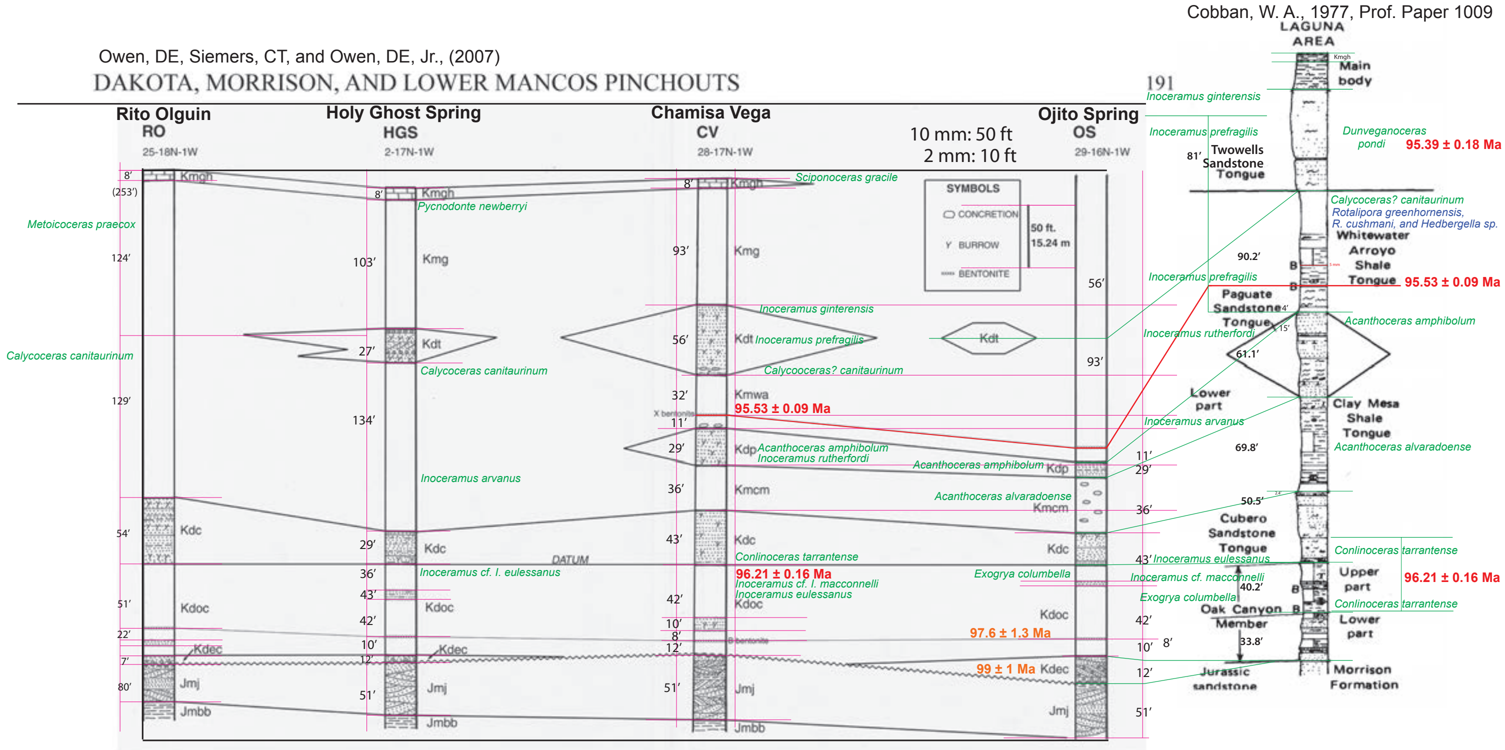

FIGURE 3. Stratigraphic cross-section from RO in La Ventana Quadrangle across Holy Ghost Spring Quadrangle, to OS in Ojito Spring Quadrangle. Abbreviations of measured sections and stratigraphic units same as on Figure 1 and 2 plus Kmg = Graneros Shale, Kmwa = Whitewater Arroyo Shale, Kmcm = Clay Mesa Shale, and Jmbb = Brushy Basin Member of Morrison Formation. 99 ± 1 and 97.6 ± 1.3 Ma Laserchron Ages from Lawton, T.F., et al., 2020

Figure S14. Middle Cenomanian ammonite/inoceramid faunas are present in the the southeast San Juan Basin (Owen et al., 2007) and adjoining Laguna Pueblo area (Cobban, 1977) that allow ages for the Thatcher fauna (96.21 ± 0.16 Ma; Batenburg et al., 2016) with *Conlinoceras tarranetense* and *Inoceramus eulessanus*; this is earliest Middle Cenomanian ammonite zone in the US Western Interior sequence, and occurs in the upper Oak Canyon Member and the Cubero Sandstone Tongue of the Dakota Sandstone. The Paguate Sandstone Tongue has both *Acanthoceras amphibolum* and *Inoceramus rutherfordi*, and the X bentonite dated at 95.53 ± 0.09 Ma occurs just 11 ft above the Paguate in the Whitewater Arroyo Shale Tongue (Owen et al., 2007), which contains *Inoceramus arvanus*. The Whitewater Arroyo Shale Tongue at Laguna also has the planktonic foraminifera index species *Rotalipora greenhornensis* and *Rotalipora cushmani* (Carey, 1992). The fossils and the dated bentonites at Laguna indicate nearly the full range of the Middle Cenomanian in the intertonguing Mancos Shale and Dakota Sandstone tongues in central New Mexico. Recent LA-ICP-MS dating of zircons presented in Lawton et al. (2020), though low precision, provides ages for the lower Oak Canyon Member of 97.6 ± 1.3 Ma and 99 ± 1 Ma for the basal Dakota Encinal Canyon Member from the same southeast San Juan Basin area; an age of 101 ± 2 was obtained on the Beartooth Quartzite in the Burro Mountains of southernmost New Mexico, similar in age to the Muddy Sandstone in Wyoming. $^{40}Ar/^{39}Ar$ ages reported with ± 2σ analytical plus J value uncertainties.

Elder, W.P., Gustason, E.R., and Sageman, B.B., 1994, Correlation of basinal carbonate cycles to nearshore parasequences in the Late Cretaceous Greenhorn seaway, Western Interior USA: Geological Society of America Bulletin, v. 106, p 892-902

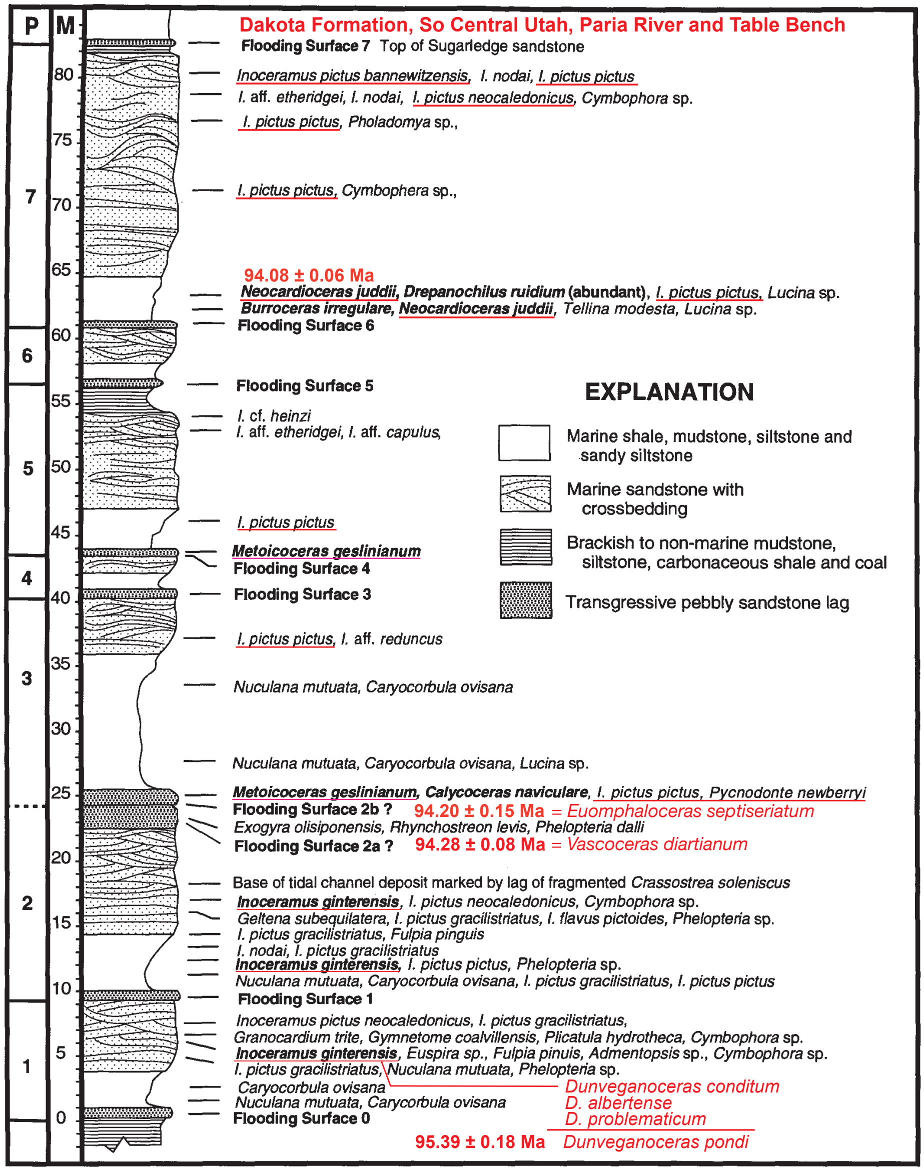

Figure 6. Composite section of study interval in the upper unit of the Dakota Formation showing lithofacies and faunal control at the Paria River (parasequences 1 and 2) and Table Bench (parasequences 3–7) sections (sections 9 and 3, respectively, Figs. 1 and 3), Utah. Biostratigraphically important taxa and flooding surfaces are labeled in bold typeface. Similar levels of biostratigraphic control are present at other Dakota sections. P = parasequence, M = meters.

Based upon: Gustason, E.R., 1989, Stratigraphy and sedimentology of the middle Cretaceous Dakota Formation, southwestern Utah [Ph.D. dissertation]: Boulder, University of Colorado

898 Geological Society of America Bulletin, July 1994

Figure S15. Upper Cenomanian ammonite/inoceramid faunas are present in south central Utah, as documented by Elder, Gustason, and Sageman (1994). Inoceramid faunas range from *Inoceramus ginterensis* up through *Inoceramus pictus*. Ammonites parallel the inoceramid biostratigraphy, including *Metoicoceras geslianum*, equivalent to Vascoceras diartianum (94.28 ± 0.08 Ma) and *Euomphaloceras septiseriatum* (94.20 ± 0.15 Ma; both ages from Meyers et al., 2012); and up to the "B" bentonite, Neocardioceras juddii zone, recently dated in southern Utah at 94.08 ± 0.06 Ma (Jones et al., 2020). The Dakota Sandstone was deposited in southern Utah across the entire upper Cenomanian, nearly to the Cenomanian-Turonian boundary. $^{40}Ar/^{39}Ar$ ages reported with ± 2σ analytical plus J value uncertainties.

Reference cited in Supplementary Materials Figures

Batenburg, S.J., De Vleeschouwer, D., Sprovieri, M., Hilgen, F.J., Gale, A.S., Singer, B.S., Koeberl, C., Coccioni, R., Claeys, P., and Montanari, A., 2016, Orbital control on the timing of oceanic anoxia in the Late Cretaceous: Climate of the Past Discussions, https://doi.org/10.5194/cp-12-1995-2016.

Carey, M.A., 1992. Upper Cenomanian Foraminifers from the southern part of the San Juan Basin, New Mexico: U.S. Geological Survey Bulletin 1808-N, p. 1-17, with 3 plates.

Cobban, W. A., 1977, Characteristic Marine Molluscan Fossils from the Dakota Sandstone and Intertongued Mancos Shale, West Central New Mexico: U.S. Geological Survey Professional Paper 1009, 30 pp.

Cobban, W.A., Erdmann, C.E., Lemke, R.W., and Maughan, E.K., 1976, Type sections and stratigraphy of the Members of the Blackleaf and Marias River Formations (Cretaceous) of the Sweetgrass Arch, Montana: U.S. Geological Survey Professional Paper 974, 71 p.

Elder, W.P., Gustason, E.R. and Sageman, B.B., 1994, Correlation of basinal carbonate cycles to nearshore parasequences in the Late Cretaceous Greenhorn seaway, Western Interior USA. Geological Society of America Bulletin, 106(7), 892-902.

Dresser, H.W., 1974, Muddy Sandstone-Wind River Basin. American Associateion of Petroleum Geologists, Earth Science Bulletin 7, No. 1, p. 5-70.

Finn, T., 2014. *Lower Cody Shale (Niobrara Equivalent) in the Bighorn Basin, Wyoming and Montana—Thickness, Distribution, and Source Rock Potential.* Scientific Investigations Report 2013-5138. US Geological Survey. 32 p.

Finn, T.M., 2017. Detailed Cross Sections of the Niobrara Interval of the Cody Shale in the Bighorn Basin, Wyoming and Montana. USGS Scientific Investigations Map 3370.

Jones, M.M., Sageman, B.B., Selby, D., Jicha, B.R., Singer, B.S., and Titus, A.L., 2020, Regional chronostratigraphic synthesis of the Cenomanian-Turonian Oceanic Anoxic Event 2 (OAE2) interval, Western Interior Basin (USA): New Re-Os chemostratigraphy and $^{40}Ar/^{39}Ar$ geochronology: Geological Society of America Bulletin, https://doi.org/10.1130/B35594.1

Lawton, T.F., Amato, J.M., Machin, S.E.K., Gilbert, J.C., and Lucas, S.G., 2020, Transition from Late Jurassic Rifting to middle Cretaceous dynamic foreland, southwestern U.S. and northwestern Mexico: Geological Society of America Bulletin, https://doi.org/10.1130/B35433.1

MacKenzie, D.B., 1965. Depositional environments of Muddy Sandstone, western Denver basin, Colorado. AAPG Bulletin, *49*(2), p.186-206.

Oboh-Ikuenobe, F., Holbrook, J.M., Scott, R.W., Akins, S.L., Evetts, M.J., Benson, D.G. and Pratt, L.M., 2008. Anatomy of Epicontinental Flooding: Late Albian-Early Cenomanian of the Southern US Western Interior Basin. Geological Association of Canada Special Paper 48, p. 201-227

Owen, DE, Siemers, CT, and Owen, DE, Jr, 2007, Dakota and adjacent lower Mancos Stratigraphy (Cretaceous and Jurassic) in the Holy Ghost Spring Quadrangle, Land of Pinchouts Jemez and Zia Indian Reservations, New Mexico: New Mexico Geological Society Guidebook 58, p. 188-194

Reeside, J.B., Jr., and Cobban, W.A., 1960, Studies of the Mowry Shale and contemporary Formations in the United States and Canada: U.S. Geological Survey Professional Paper 355, 237 p.

Richards, P.W., 1955. *Geology of the Bighorn Canyon-Hardin Area, Montana and Wyoming*. USGS Bulletin 126, US Government Printing Office, 93 pp.

Robinson, C.S., Mapel, W.J. and Bergendahl, M.H., 1964. *Stratigraphy and structure of the northern and western flanks of the Black Hills uplift, Wyoming, Montana, and South Dakota.* USGS Professional Paper 404, 134 pp.

Table S2. **Complete U-Pb isotopic data from zircons and concordia plots from Dakota Sandstone, Dinosaur Ridge, Jefferson County, Colorado**

	Composition			*Isotopic Ratios*								*Dates*						
Fraction	**Th/U** (a)	**Pbc** (b) [pg]	**Pb*/Pbc** (c)	^{206}Pb/^{204}Pb (d)	^{208}Pb/^{206}Pb (e)	^{206}Pb/^{238}U (e,f)	±2σ [%]	^{207}Pb/^{235}U (e)	±2σ [%]	^{207}Pb/^{206}Pb (e,f)	±2σ [%]	^{206}Pb/^{238}U (f,g)	±2σ [abs.]	^{207}Pb/^{235}U (g)	±2σ [abs.]	^{207}Pb/^{206}Pb (f,g)	±2σ [abs.]	Corr. coef.
KJ08-160: Zircon																		
z3	0.47	0.43	21	1275	0.149	0.016374	0.094	0.10967	1	0.048602	0.986	104.70	0.10	105.7	1	128	23	0.35
z4	0.53	0.59	9	576	0.169	0.01637	0.18	0.10889	2.2	0.048268	2.19	104.67	0.19	105	2.2	111	52	0.34
z5	0.51	0.52	18	1111	0.163	0.01637	0.11	0.10898	1.1	0.048307	1.11	104.67	0.11	105	1.1	113	26	0.39
z6	0.64	1.1	9	521	0.203	0.016373	0.21	0.10934	2.5	0.048457	2.45	104.69	0.22	105.4	2.5	121	58	0.37
z7	0.49	1.67	10	617	0.156	0.016372	0.17	0.10938	2.1	0.048477	2.04	104.69	0.18	105.4	2.1	122	48	0.32
z9	0.54	0.49	35	2067	0.173	0.016372	0.1	0.10873	0.66	0.048186	0.627	104.69	0.11	104.8	0.66	107	15	0.43
KJ08-161: Zircon																		
z4	0.45	0.54	9	577	0.143	0.016258	0.19	0.10827	2.3	0.048322	2.25	103.96	0.20	104.4	2.3	114	53	0.27
z6	0.39	0.93	17	1069	0.125	0.016261	0.12	0.10861	1.2	0.048462	1.18	103.98	0.13	104.7	1.2	121	28	0.24
z8	0.34	1.6	5	307	0.109	0.016272	0.37	0.10992	4.3	0.049016	4.21	104.05	0.39	105.9	4.3	148	99	0.35
z9	0.58	0.8	30	1767	0.184	0.016266	0.088	0.10819	0.76	0.048264	0.727	104.01	0.09	104.31	0.75	111	17	0.39
z10	0.34	1.3	18	1108	0.109	0.016265	0.11	0.10856	1.2	0.048429	1.12	104.00	0.11	104.6	1.1	119	26	0.33
z11	0.37	0.63	26	1614	0.117	0.016265	0.12	0.10787	0.88	0.048124	0.851	104.01	0.12	104.02	0.87	104	20	0.29
z12	0.44	0.67	22	1336	0.142	0.016254	0.11	0.10794	1	0.048183	1.02	103.94	0.11	104.1	1	107	24	0.33
z17	0.43	0.67	24	1481	0.138	0.016272	0.11	0.10866	0.91	0.048454	0.864	104.05	0.11	104.74	0.9	120	20	0.45
z20	0.38	2.69	6	357	0.122	0.016267	0.32	0.10995	3.7	0.049043	3.56	104.02	0.33	105.9	3.7	149	83	0.35
KJ08-162: Zircon																		
z1	0.37	0.57	49	3014	0.117	0.016252	0.074	0.10813	0.49	0.048275	0.46	103.92	0.08	104.25	0.49	112	11	0.45
z3	0.44	0.44	25	1535	0.139	0.016253	0.097	0.10861	0.91	0.048488	0.89	103.93	0.10	104.7	0.91	122	21	0.27
z6	0.35	0.46	30	1879	0.111	0.016249	0.084	0.10805	0.68	0.048247	0.67	103.91	0.09	104.18	0.67	110	16	0.19
z8	0.37	0.72	20	1226	0.119	0.016248	0.13	0.10793	1.1	0.048197	1	103.90	0.14	104.1	1.04	108	24	0.42
z9	0.42	0.94	18	1127	0.134	0.016252	0.12	0.10816	1.2	0.048287	1.1	103.93	0.12	104.3	1.16	112	27	0.28

Blank composition: ^{206}**Pb**/^{204}**Pb** = 18.15 ± 0.48; ^{207}**Pb**/^{204}**Pb** = 15.30 ± 0.29; ^{208}**Pb**/^{204}**Pb** = 37.11 ± 0.88; Mass fractionation correction of 0.25%/amu±0.02%/amu (atomic mass unit) was applied to all single-collector Daly analyses.

(a) Th contents calculated from radiogenic ^{208}**Pb** and the ^{207}**Pb**/^{206}**Pb** date of the sample, assuming concordance between U-Th and Pb systems.

(b) Total mass of common Pb.

(c) Ratio of radiogenic Pb (including ^{208}**Pb**) to common Pb.

(d) Measured ratio corrected for fractionation and spike contribution only. All common Pb was assumed to be procedural blank. Total procedural blank for U was less than 0.1 pg.

(f) Corrected for Initial Th/U disequilibrium using radiogenic ^{208}**Pb** and Th/U [magma] = 2.8

(g) Isotopic dates calculated using the decay constants λ_{238} = 1.55125E-10 yr^{-1}, λ_{235} = 9.8485E-10 yr^{-1} (Jaffey et al. 1971), and for the ^{238}**U**/^{235}**U** = 137.818 ± 0.045 (Hiess, J. et al. 2012)